L1(0) ordering and magnetic interactions in FePt nanoparticles embedded in MgO and SiO2 shell matrices

Tomou, Aphrodite; Panagiotopoulos, Ioannis; Gournis, Dimitrios; Kooi, Bart

Published in:
Journal of Applied Physics

DOI:
10.1063/1.2752141

$L1_0$ ordering and magnetic interactions in FePt nanoparticles embedded in MgO and SiO_2 shell matrices

Aphrodite Tomou, Ioannis Panagiotopoulos,[a),b)] and Dimitrios Gournis[a),c)]
Department of Materials Science and Engineering, University of Ioannina, Ioannina 45110, Greece

Bart Kooi
Zernike Institute for Advanced Materials, University of Groningen, Nijenborgh 4, 9747 AG Groningen, The Netherlands

(Received 6 February 2007; accepted 25 May 2007; published online 24 July 2007)

FePt nanoparticles have been encapsulated in insulating and protective MgO shells, using a two step chemical process, in order to prevent sintering during the heat-treatment process required for the $L1_0$ ordering. The FePt nanoparticles were initially prepared using a standard polyol process and then dispersed in a magnesium oxide solution. As a basis for comparison FePt/SiO_2 nanocomposites have been also synthesized using a modified aqueous sol-gel route as the second step. The magnetic and microstructural properties of FePt/MgO and FePt/SiO_2 nanocomposites are compared with those of FePt nanoparticles. The presence of oxide matrices leads to more homogeneous microstructures and better magnetic properties. While higher coercivity values have been obtained in FePt/SiO_2, the MgO matrix is proven to provide better physical and magnetic isolations of the FePt nanoparticles. However, for FePt:MgO molar ratios exceeding 1:20 no $L1_0$ ordering has been achieved. © *2007 American Institute of Physics*. [DOI: 10.1063/1.2752141]

I. INTRODUCTION

Magnetic nanoparticles are interesting from both the applied and fundamental points of view, as their properties differ from those of bulk materials due to the increased fraction of surface atoms. However, for any ferromagnetic material there is a critical particle size below which thermal fluctuations become dominant leading to a superparamagnetic behavior, resulting in a loss of any permanent magnetization. Chemically synthesized self-assembled ferromagnetic FePt nanoparticles have been proposed as candidates for the next generation ultrahigh-density magnetic recording media as well as for nanocomposite high energy product permanent magnets due to their high magnetocrystalline anisotropy which inhibits thermal demagnetization at room temperature down to particle sizes of about 2–4 nm.[1,2] The as-synthesized particles are usually produced in the chemically disordered structure (face centered cubic $A1$) and a heat treatment is needed for the transformation to the chemically ordered high anisotropy FePt structure (face centered tetragonal $L1_0$).[3] Thus, despite the initial enthusiasm that followed the report on the chemical preparation of superlattices of monodispersed FePt nanoparticles for high-density magnetic recording media,[1] a major limitation to their practical application was soon recognized: The required heat-treatment process leads to sintering effects and the loss in particle positional order[3–5] destroying their major advantage of superior microstructural uniformity. Additives such as Ag, Sb, Au, etc., have been shown to significantly reduce the required annealing temperature[6–10] but on the other hand they tend to favor grain growth. Grain growth inhibitors on the other hand tend to increase the ordering temperature. A possible route to prevent coalescence is by the implementation of polymer-assisted assembly methods.[11,12] Furthermore heat treatment in a forming gas (5% H_2 in N_2) has been shown to yield faster $L1_0$ ordering compared to that obtained after vacuum annealing.[13,14]

Another approach to tackle this problem is to embed the nanoparticles in appropriate nonmagnetic matrices.[15] Several works have focused on the preparation of core-shell morphologies in which the magnetic FePt core is surrounded by an oxide shell (SiO_2,[16–18] TiO_2,[19] MnO,[20] and Fe_xO_y[21,22]) which prevents sintering. Nonmagnetic shells are preferable since they also provide the magnetic isolation required in magnetic recording applications.

A similar approach has been used to make granular films of FePt/Al_2O_3,[23] FePt/MgF_2,[23] CoCrPt/SiO_2,[24] and FePt/MgO.[25,26] MgO can serve as a shell matrix since it hinders the aggregation of the metal particles and can be dissolved from the nanocomposite using low concentration acid solutions (e.g., HCl), leaving the structural characteristics of the magnetic nanoparticles almost intact.[27] The chemical synthesis of FePt nanoparticles embedded in the MgO matrix has not been reported. Here we evaluate the effectiveness of chemically synthesized MgO shells, in comparison with FePt/SiO_2 (synthesized according to Ref. 17), as a means to provide sintering prevention and magnetic isolation of FePt nanoparticles produced by the standard polyol method. Note that the nanoparticles are heat-treated and studied in powder form, which facilitates agglomeration and sintering compared to being spread on substrates.

II. EXPERIMENTAL DETAILS

Platinum acetylacetonate (97%), cobalt acetate (99.995%), diphenylether (99%), 1,2-dodecanediol (90%),

[a)]Authors to whom correspondence should be addressed.
[b)]FAX: +30 26510 97074; electronic mail: ipanagio@cc.uoi.gr
[c)]FAX: +30 26510 97074; electronic mail: dgourni@cc.uoi.gr

oleylamine (70%, technical grade), oleic acid (90%, technical grade), and magnesium oxide and tetraethyl orthosilicate 98% (TEOS) were supplied from Sigma-Aldrich. Absolute ethanol and acetone were obtained from Riedel-de Haën. *n*-hexane (95%) was purchased from Lab-Scan analytical sciences. Ammonium hydroxide solution was ordered from Fluka. All chemicals were used as received.

Monodispersed FePt nanoparticles were prepared by the polyol synthetic procedure: Diphenylether (20 ml), 1,2-dodecanediol (10 mmol), and oleylamine (5 mmol) were mixed in a spherical flask (50 ml) and refluxed under vigorous stirring at 140 °C for 10 min. Platinum (II) acetylacetonate (1 mmol), iron pentacarbonyl (2 mmol), and oleic acid (5 mmol) were then added to the solution. The temperature was raised up to 180 °C and kept there for 3 h after which the heat source was removed and the mixture was allowed to cool to room temperature. The resultant FePt nanoparticles were then precipitated with absolute ethanol (40 ml) and isolated by centrifugation. The precipitates were washed twice with ethanol and centrifuged and the final FePt precipitate was dispersed with acetone and then dried at room temperature.

The FePt/MgO nanocomposites were prepared as follows: MgO (2–20 mmol) was dispersed into the nonpolar solvent *n*-hexane (4 ml) and the suspension was stirred and sonicated for 80 min. FePt nanoparticles (25 mg) in *n*-hexane (4 ml) were then added to the previous suspension. The final mixture was stirred and sonicated alternatively for 80 min in total. Then, the suspension was stirred for another 12 h and finally dried at room temperature.

For the preparation of $FePt/SiO_2$ nanocomposites the following sol-gel process, based on Ref. 17 was used: FePt nanoparticles (25 mg) in *n*-hexane (3.5 ml) were added to a TEOS (0.1 ml) solution in ethanol (20 ml) under sonication and vigorous stirring. The ammonium hydroxide solution (1.5 ml) was then added slowly to the mixture and stirred for 3 h. The resultant $FePt/SiO_2$ particles were separated by centrifugation and washed several times with ethanol in order to remove the excess of silica formed during the hydrolysis condensation. Finally the sample was dried at room temperature.

FePt/MgO and $FePt/SiO_2$ were sealed in evacuated quartz tubes and annealed. FePt nanoparticles are typically annealed at temperatures in the range of 550–800 °C.[3,28] Lower temperatures lead to incomplete ordering resulting in low coercivities. In our samples no significant coercivity has been obtained for heat-treatment temperatures below 650 °C. In order to check the effectiveness of the cell matrices we have chosen to compare samples heat-treated at 700 and 750 °C for different times ranging from 10 min to 3 h. X-ray powder diffraction data were collected using a D8 Advance Bruker diffractometer by using Cu $K\alpha$ radiation and a secondary beam graphite monochromator. The patterns were recorded in the 2-theta (2θ) range from 2° to 100°, with steps of 0.02° and a counting time of 2 s per step. Magnetic measurements were carried out using a vibrating-sample magnetometer (VSM) (Lakeshore 3700).

Transmission electron micrographs were obtained using a JEOL JEM-2010F microscope (operating at 200 kV) equipped with an EDAX detector. For the preparation of transmission electron microscope (TEM) samples a drop of the corresponding nanoparticle solution in hexane was deposited onto a holey-carbon coated copper grid and left to evaporate.

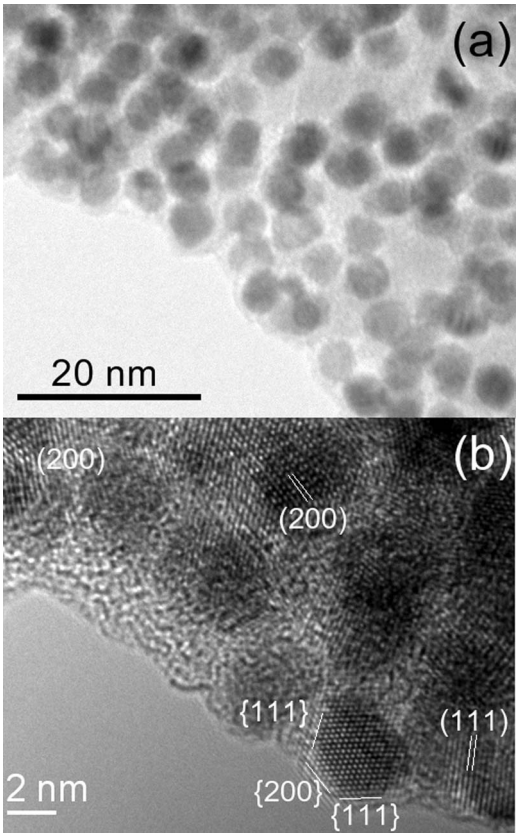

FIG. 1. (a) TEM (bright field) and (b) HRTEM images of as prepared FePt/MgO nanocomposites.

III. RESULTS AND DISCUSSION

Figure 1 shows TEM images of the as-prepared FePt/MgO nanocomposites. The (111) and (200) planes of the cubic FePt *A*1 structure are commonly observed in the high resolution TEM (HRTEM) images of these samples. In a few cases nanocrystals having a polyhedral shape with specific facets have been identified.[5] The oxide appears as a shell surrounding the FePt particles in a homogeneous microstructure. Due to the high density of the particles the shells appear coalesced into a continuous matrix. An average particle size of 4.3 nm and a standard deviation of 0.6 nm have been calculated by performing statistics on 100 different particles.

Figure 2 shows similar TEM images for the $FePt/SiO_2$ nanocomposites: An average size of 4.3 nm and a standard deviation of 0.4 nm have been calculated.

Hysteresis loops of heat treated FePt nanoparticles are shown in Fig. 3 and compared with those of FePt/MgO and $FePt/SiO_2$ nanocomposites. The loops of FePt nanoparticles and FePt/MgO nanocomposites heat-treated at 700 °C are smooth and have coercivities (H_C) of 5.9 and 6.5 kOe, respectively [Fig. 3(a)]. An important parameter for recording

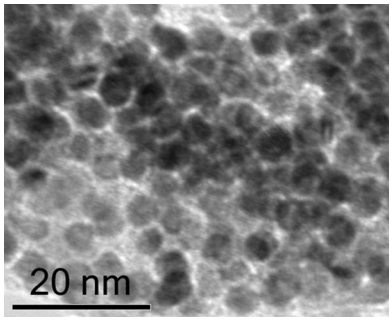

FIG. 2. TEM bright-field image of an as prepared FePt/SiO2 nanocomposite.

applications is the coercivity squareness S^* that characterizes the steepness of the demagnetization curve at H_C and can be defined as[29]

$$S^* = 1 - \frac{M_R}{H_C} \frac{1}{dM/dH|_{H_C}}.$$

Apart from a small difference in H_C the loop shapes of FePt and FePt/MgO look quite similar at first sight. However, the composite shows a substantially higher $S^*=0.5$ compared to just $S^*=0.1$ for the FePt. For the $FePt/SiO_2$ nanocomposite a similar H_C is obtained but the hysteresis loop shows a constricted shape which usually indicates a heterogeneous nature incorporating uncoupled phases of different magnetic hardness. This constricted loop shape could arise due to the excessive grain growth leading to multidomain particles and/or incomplete transformation leading to the existence of phases with different degrees of ordering. In FePt nanoparticles the mechanisms of $L1_0$ ordering and grain growth are combined[30] and therefore the magnetic properties are expected to depend very sensitively on the initial particle size and microstructure as well as on the ordering and sintering effects during the heat-treatment process. The differences between the composite samples and the single FePt nanoparticles become more obvious at higher annealing temperatures. The loops after heat treatment at 750 °C for 10 min are presented in Fig. 3(b). The FePt sample loop has a constricted shape typical of overaging while the FePt/MgO preserves a smooth loop shape with $H_C=6$ kOe and $S^*=0.5$. For the SiO_2 composite a high $H_C=13$ kOe is obtained but a step around the field reversing point indicates the coexistence of a softer phase. From the x-ray diffraction (XRD) patterns the c/a ratio of the tetragonal cell can be calculated which gives a measure of the degree of ordering to the $L1_0$ structure. It is 0.968 for the bare FePt nanoparticles, 0.970 for $FePt/SiO_2$, and 0.973 for the FePt/MgO. For the shake of comparison note that the bulk value (JCPD No. 43-1359) is 0.964. Thus though some differences in the degree of ordering do exist, they are not very large and the difference in microstructural characteristics may be more crucial in determining the magnetic response. In the case of SiO_2 based composites, the asymmetry between the field increasing and field decreasing braches of the hysteresis loops, as well as the fact that the loop does not close after a hysteresis cycle has been traced [Fig. 3(b)], indicates the existence of very high anisotropy regions that cannot be switched within the maximum field of 20 kOe.

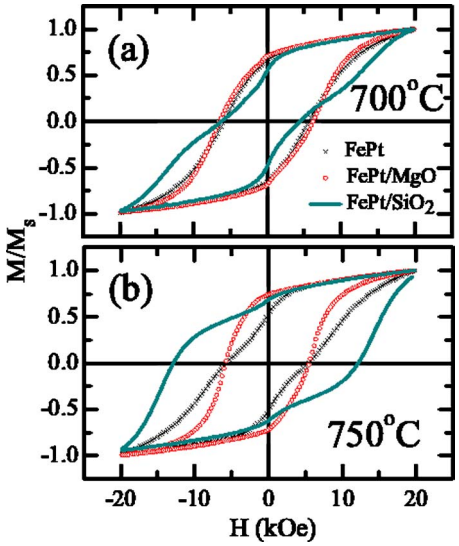

FIG. 3. (Color online) Hysteresis loops of heat-treated FePt nanoparticles and FePt/MgO and $FePt/SiO_2$ nanocomposites: (a) at 700 °C for 30 min and (b) at 750 °C for 30 min.

It is known that the H_C is maximized for isolated particles with a size approaching the single domain size. When either this size is exceeded or strong interparticle interactions are present, nonhomogeneous rotation mechanisms set in reducing H_C. The effectiveness of each matrix in providing magnetic isolation between the grains can be checked by the construction of δM plots which are widely used to characterize magnetic interactions in recording media.[31] These are defined as

$$\delta M(H) = 2M_R(H) + M_D(H) - 1,$$

where $M_R(H)$ is the isothermal remanent magnetization curve, obtained after the successive application and removal of positive magnetizing fields H on a thermally demagnetized sample, and $M_D(H)$ is the dc demagnetization remanence curve, obtained by successively applying and removing reversed fields $-H$ on a previously positively saturated sample. Positive δM values are attributed to magnetizing exchange interactions, while negative ones to dipolar interactions and the presence of soft phases.

The δM plots are shown in Fig. 4. The plot of the heat-treated FePt nanoparticle system is characterized by strong exchange interactions in the whole field range with a maximum at H_C indicating particle coalescence. In the case of $FePt/SiO_2$ nanocomposites the positive part (maximized at H_C) appears to be superimposed on a large negative contribution usually observed in isolated nanoparticles.[3,7] A more effective reduction of the magnetic interactions is achieved in the FePt/MgO composites both in terms of the height as well as the width of the positive contribution. The latter reflects a narrower switching field distribution probably related to the increased S^*.

A characteristic example of the sintering prevention achieved is presented in Fig. 5 where the TEM images of heat-treated $FePt/SiO_2$, FePt/MgO, and FePt samples at 700 °C are compared. Both $FePt/SiO_2$ and FePt/MgO composites are characterized by a particle size of the order of

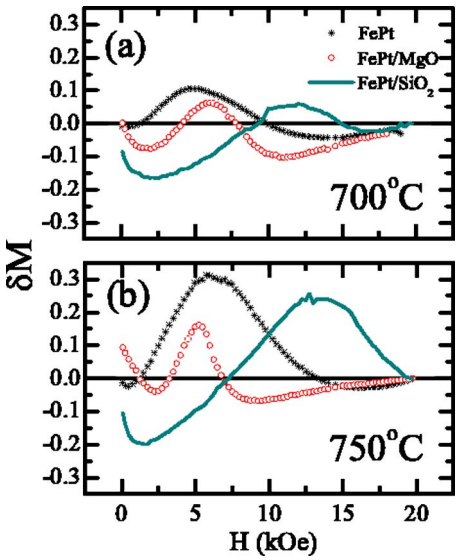

FIG. 4. (Color online) δM plots of heat-treated FePt nanoparticles and FePt/MgO and FePt/SiO_2 nanocomposites: (a) at 700 °C for 30 min and (b) at 750 °C for 30 min.

5–10 nm. After the heat treatment, the FePt nanoparticle system shows a very heterogeneous structure comprising particles with sizes ranging from 5 to 50 nm. In contrast, the composites retain a much more uniform microstructure. For instance, for the heat-treated FePt/MgO one can derive an average 5.6±1.7 nm, in comparison with 4.6±0.6 nm for the same sample before the heat treatment.

Lastly we discuss the effect of the oxide matrix content. Increasing the oxide matrix volume is obviously favorable for particle isolation. On the other hand the kinetics of $L1_0$ ordering are substantially influenced by the particle size[10,32,33] when the particles become completely separated. In Fig. 6 the XRD patterns of heat-treated FePt/MgO composites prepared with different FePt to MgO molar ratios are compared. In each experiment 25 mg of FePt was used, corresponding to 0.1 mmol which was mixed with 2–20 mmol of MgO. The microstructural heterogeneity of the MgO-free FePt sample is so strong that it can be seen even in the XRD pattern profiles. In order to analyze the peak profiles one has to consider two overlapping peaks of different half widths corresponding to "Scherrer" particle sizes of 6 and 32 nm. At low MgO concentration (2 mmol) the FePt is ordered in the $L1_0$ phase. The particle size is estimated at 18 nm and MgO peaks are not identified. For 6 mmol of MgO, matrix peaks appear that correspond to a structural coherence length of 34 nm while the FePt particle size is estimated to be 7 nm. No superstructure peak is observed which indicates that at such reduced particle sizes the FePt phase cannot be ordered but instead remains in the cubic structure. Similar observations hold for the 20 mmol MgO sample for which a MgO structural coherence length around 34 nm is also found while the FePt particle size is estimated at only 5 nm which coincides with the as-prepared particle size. Such particle size effects have been previously reported in similar FePt nanoparticle systems and the critical sizes are found to be system

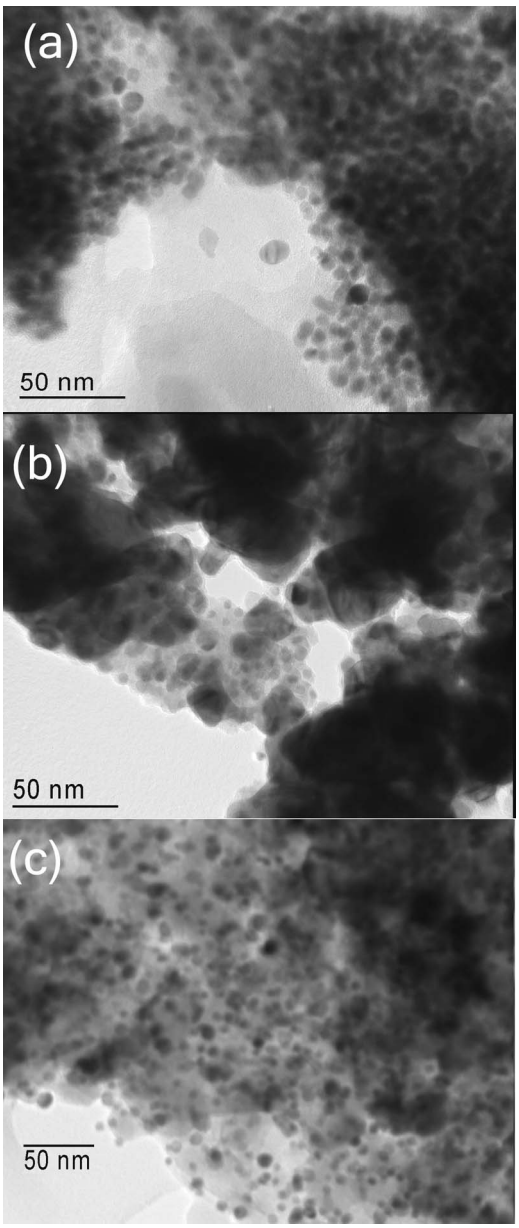

FIG. 5. TEM bright-field images of heat-treated (a) FePt/SiO_2 nanocomposite, (b) FePt nanoparticles, and (c) FePt/MgO nanocomposite.

dependent. This is attributed to differences in the interfacial energies and the fact that the interfacial disorder hinders the $L1_0$ ordering.[33] Furthermore, close to the critical particle size for chemical ordering, a higher annealing temperature is required. In our case the displacement of the FePt (111) peak for the 6 mmol MgO sample reveals a change of the chemical composition towards a higher Pt content. A composition near $Fe_{40}Pt_{60}$ can be estimated which lies within the cubic $FePt_3$ phase boundary. This may explain the lack of $L1_0$ ordering despite the fact that the 5 nm particle size is above the theoretically predicted required minimum of 2–3 nm.[32] The reason for this stoichiometry change is not clear. Preferential Fe oxidation at the FePt/MgO interface is a possible cause.

IV. SUMMARY AND CONCLUSIONS

In conclusion, FePt/MgO nanocomposites have been prepared by a two-step chemical synthesis process involving

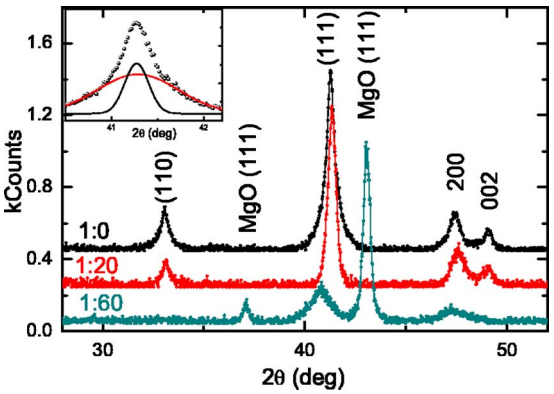

FIG. 6. (Color online) XRD patterns of heat-treated FePt/MgO nanocomposites compared to those of FePt nanoparticles. The peaks are indexed to the tetragonal $L1_0$ structure or the cubic MgO structure where indicated. The numbers on the left indicate FePt:MgO molar ratios used during the preparation, thus 1:0 denotes stand-alone FePt nanoparticles. The inset shows an enlarged graph of the (111) peak profile of the heat-treated stand-alone FePt and its analysis to two components corresponding to different Scherrer sizes.

polyol synthesis of FePt nanoparticles and their dispersion in oxide containing solutions. For comparison, a sol-gel method was used to produce $FePt/SiO_2$. The oxide matrices provide sintering prevention during the required heat-treatment process and lead to more homogeneous microstructures and better magnetic properties. While higher H_C values have been obtained for $FePt/SiO_2$, the MgO matrix is proven to provide better physical and magnetic isolations of the FePt nanoparticles. At high FePt:MgO molar ratios, exceeding 1:20, $L1_0$ ordering and H_C development are hindered. This is related to stoichiometry changes of the metallic phase and must not be attributed to the reduced particle size, which is still safely above the critical value for $L1_0$ ordering. Better isolation of magnetic nanoparticles in the FePt/MgO system in conjunction with the advantages that arise from the use of MgO render these nanocomposites as attractive candidates for magnetic recording media.

ACKNOWLEDGMENTS

Thanks are due to T. Tsoufis for his help with laboratory work. This research was supported in part by the IKYDA 2005 program No95. The authors acknowledge the Network of Laboratory Units and Centers of the University of Ioannina for the use of the VSM and XRD facilities.

[1] S. H. Sun, C. B. Murray, D. Weller, L. Folks, and A. Moser, Science **287**, 1989 (2000).
[2] K. E. Elkins, T. S. Vedantam, J. P. Liu, H. Zeng, S. H. Sun, Y. Ding, and Z. L. Wang, Nano Lett. **3**, 1647 (2003).
[3] H. Zeng, S. H. Sun, T. S. Vedantam, J. P. Liu, Z. R. Dai, and Z. L. Wang, Appl. Phys. Lett. **80**, 2583 (2002).
[4] Z. R. Dai, S. H. Sun, and Z. L. Wang, Nano Lett. **1**, 443 (2001).
[5] Z. R. Dai, S. H. Sun, and Z. L. Wang, Surf. Sci. **505**, 325 (2002).
[6] S. Kang, J. W. Harrell, and D. E. Nikles, Nano Lett. **2**, 1033 (2002).
[7] S. Wang, S. S. Kang, D. E. Nikles, J. W. Harrell, and X. W. Wu, J. Magn. Magn. Mater. **266**, 49 (2003).
[8] Q. Y. Yan, T. Kim, A. Purkayastha, P. G. Ganesan, M. Shima, and G. Ramanath, Adv. Mater. (Weinheim, Ger.) **17**, 2233 (2005).
[9] J. W. Harrell *et al.*, Scr. Mater. **53**, 411 (2005).
[10] C. Srivastava, G. B. Thompson, J. W. Harrell, and D. E. Nikles, J. Appl. Phys. **99**, 054304 (2006).
[11] S. H. Sun *et al.*, J. Am. Chem. Soc. **124**, 2884 (2002).
[12] S. H. Sun, S. Anders, T. Thomson, J. E. E. Baglin, M. F. Toney, H. F. Hamann, C. B. Murray, and B. D. Terris, J. Phys. Chem. B **107**, 5419 (2003).
[13] T. S. Vedantam, J. P. Liu, H. Zeng, and S. Sun, J. Appl. Phys. **93**, 7184 (2003).
[14] H. L. Wang, Y. Huang, Y. Zhang, G. C. Hadjipanayis, D. Weller, and A. Simopoulos, J. Magn. Magn. Mater. **310**, 22 (2007).
[15] D. R. Li, N. Poudyal, V. Nandwana, Z. Q. Jin, K. Elkins, and J. P. Liu, J. Appl. Phys. **99**, 08E911 (2006).
[16] Y. Ding, S. A. Majetich, J. Kim, K. Barmak, H. Rollins, and P. Sides, J. Magn. Magn. Mater. **284**, 336 (2004).
[17] M. Aslam, L. Fu, S. Li, and V. P. Dravid, J. Colloid Interface Sci. **290**, 444 (2005).
[18] S. Yamamoto, Y. Morimoto, T. Ono, and M. Takano, Appl. Phys. Lett. **87**, 032503 (2005).
[19] J. Sort *et al.*, Adv. Mater. (Weinheim, Ger.) **18**, 466 (2006).
[20] S. S. Kang, G. X. Miao, S. Shi, Z. Jia, D. E. Nikles, and J. W. Harrell, J. Am. Chem. Soc. **128**, 1042 (2006).
[21] M. Chen, J. P. Liu, and S. H. Sun, J. Am. Chem. Soc. **126**, 8394 (2004).
[22] C. Liu, X. W. Wu, T. Klemmer, N. Shukla, and D. Weller, Chem. Mater. **17**, 620 (2005).
[23] Y. K. Takahashi, T. Ohkubo, M. Ohnuma, and K. Hono, J. Appl. Phys. **93**, 7166 (2003).
[24] Y. F. Xu, J. P. Wang, and Y. Su, J. Phys. D **33**, 1460 (2000).
[25] T. Shima, K. Takanashi, Y. K. Takahashi, and K. Hono, Appl. Phys. Lett. **88**, 063117 (2006).
[26] Y. G. Peng, J. G. Zhu, and D. E. Laughlin, J. Appl. Phys. **99**, 08F907 (2006).
[27] T. Tsoufis, P. Xidas, L. Jankovic, D. Gournis, A. Saranti, T. Bakas, and M. A. Karakassides, Diamond Relat. Mater. **16**, 155 (2007).
[28] M. H. Lu, T. Song, T. J. Zhou, J. P. Wang, S. N. Piramanayagam, W. W. Ma, and H. Gong, J. Appl. Phys. **95**, 6735 (2004).
[29] R. L. Comstock, *Introduction to Magnetism and Magnetic Recording*, 1st ed. (Wiley, New York, 1999).
[30] T. J. Klemmer, C. Liu, N. Shukla, X. W. Wu, D. Weller, M. Tanase, D. E. Laughlin, and W. A. Soffa, J. Magn. Magn. Mater. **266**, 79 (2003).
[31] P. E. Kelly, K. Ogrady, P. I. Mayo, and R. W. Chantrell, IEEE Trans. Magn. **25**, 3880 (1989).
[32] T. Miyazaki *et al.*, Phys. Rev. B **72**, 144419 (2005).
[33] Y. K. Takahashi, T. Koyama, M. Ohnuma, T. Ohkubo, and K. Hono, J. Appl. Phys. **95**, 2690 (2004).